BIOCHEMISTRY
including biophysical chemistry & molecular biology

Article

pubs.acs.org/biochemistry

Different Molecular Mechanisms of Inhibition of Bovine Viral Diarrhea Virus and Hepatitis C Virus RNA-Dependent RNA Polymerases by a Novel Benzimidazole

Shailendra Asthana,*[,†,§] Saumya Shukla,[†] Attilio V. Vargiu,[‡] Matteo Ceccarelli,[§] Paolo Ruggerone,*[,§] Giuseppe Paglietti,[∥] Maria E. Marongiu,[†] Sylvain Blois,[†] Gabriele Giliberti,[†] and Paolo La Colla*[,†]

[†]Dipartimento di Scienze Biomediche, Università degli Studi di Cagliari, Cittadella Universitaria, 09042 Monserrato (CA), Italy
[‡]Istituto Officina dei Materiali del CNR, UOS Cagliari, Italy
[§]Dipartimento di Scienze Fisiche, Università degli Studi di Cagliari, Cittadella Universitaria, 09042 Monserrato (CA), Italy
[∥]Dipartimento di Scienze del Farmaco, Università degli Studi di Sassari, Via Muroni 23/a, 07100 Sassari, Italy

Supporting Information

ABSTRACT: The virus-encoded RNA-dependent RNA polymerase (RdRp) has emerged as a primary target in the search for selective inhibitors of Flaviviridae. Recently, we reported on the selective inhibition, in cell-based assays, of both BVDV (EC_{50} = 0.80 ± 0.06 μM) and HCV (EC_{50} = 1.11 ± 0.15 μM) by 2-{1-[2-(2,4-dimethoxyphenyl)-1*H*-benzimidazol-5-yl]-ethylidene}hydrazinecarbothioamide (227G). Here we show that, in enzyme assays with recombinant enzymes, 227G inhibits, in a dose-dependent manner, the RdRp of both BVDV (IC_{50} = 0.0020 ± 0.0004 μM) and HCV (IC_{50} = 0.40 ± 0.04 μM). Furthermore, we report on the selection and molecular analysis of a BVDV-resistant mutant, characterized by the presence of the I261M mutation. By applying a multilevel computational approach, we identified different 227G binding sites on the two RdRps. They were further validated by the good agreement between the calculated affinities and those extrapolated from IC_{50} values. Our findings suggest different molecular mechanisms of inhibition of the HCV and BVDV RdRps by 227G and indicate the importance of understanding ligand−enzyme interactions at the molecular level for the rational design of new and more potent leads.

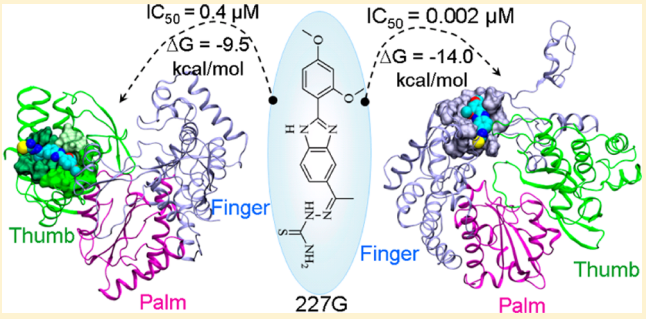

The Flaviviridae family consists of three genera: *Hepacivirus* [e.g., hepatitis C virus (HCV)], *Flavivirus* [e.g., yellow fever virus (YFV)], and *Pestivirus* [e.g., bovine viral diarrhea virus (BVDV)], all of which cause severe diseases in humans and/or animals. Worldwide, more than 170 million people are chronically infected with HCV and are at risk of developing cirrhosis and/or liver cancer.[1] Infections caused by arthropod-borne Flaviviruses are emerging throughout the world,[2,3] and those sustained by Pestiviruses have a serious impact on livestock.[4] With the exception of YFV, no vaccines are available against Flaviviridae pathogens, and selective antiviral drugs are not yet available to prevent and/or treat their infections. The sole exception is represented by HCV infections, whose standard therapy has long consisted of the administration of pegylated α-interferon (IFN-α) in combination with ribavirin.[5] This treatment is effective only in approximately half of patients and often produces toxicity and significant side effects.[6−8] Recently, two HCV protease inhibitors (PIs) have been approved, to be used in combination with IFN-α and ribavirin, for the treatment of genotype 1 chronic HCV infections.[9−12] Nevertheless, identifying new lead compounds targeted at virus-specific steps of the replication cycle of HCV as well as of other Flaviviridae remains imperative.[13−15]

Following the successful paradigm established for HIV, efforts at developing anti-Flaviviridae agents are today focused on the inhibition of essential virus-encoded enzymes.[16] In this regard, the NS3/4A helicase/NTPase and protease as well the NS5A/B RNA-dependent RNA polymerases (RdRp) appeared to be the most attractive targets for novel treatment options.[17,18]

The three-dimensional structures of RdRps from various RNA viruses are significantly similar and resemble a right hand[19−22] in which the Palm domain contains the catalytic site and the Finger and Thumb domains are responsible for the interaction with the RNA. Two Finger loops (λ1 and λ2) extend from the Finger and make contact with the Thumb, resulting in an "encircled active site" for the interaction with RNA templates.[19,20] When compared to its HCV counterpart,

Received: January 28, 2013
Revised: April 16, 2013
Published: April 29, 2013

the BVDV λ1 loop is more extended and contains a unique N-terminal domain that folds on top of the Thumb domain.[19,21,22]

On the basis of their chemical structure and mode of action, compounds targeting the RdRps can be divided into nucleoside (NI) and non-nucleoside (NNI) inhibitors, which can be used in combination to increase the effectiveness of antiviral responses across all genotypes.[23,24]

NIs, discovered through the rational search for substrate analogues, target the catalytic site,[25−28] compete with natural NTP substrates, and/or act as nonobligate "chain terminators" after incorporation into nascent RNA chains. They are effective against different genotypes and feature a relatively high barrier to drug resistance.[29−32] NNIs (which comprise the compound object of this study), discovered as HCV RdRp inhibitors in high-throughput screening programs, are structurally diverse small molecules that noncompetitively target the RdRp free of substrate and not bound to partner proteins.[3,5,15−17] By binding to allosteric cavities of the RdRp, NNIs trap the enzyme in a conformation that prevents the functional transition from the initiation to the elongation phase of transcription.[33−35]

Four NNI allosteric binding sites have been reported on the HCV RdRp, two in the Thumb and two in the Palm domains.[18,36] No structural information is available for NNIs binding to the BVDV RdRp ($RdRp_{BVDV}$), on which docking studies have identified a few and partially overlapping binding pockets, located within the Finger domain.[37−40] However, to the best of our knowledge, no study including a validation of docking results through state-of-the-art molecular dynamics (MD) simulations has been reported for NNI−$RdRp_{BVDV}$ complexes.

As far as the NNI mode of action is concerned, in HCV they prevent RNA synthesis initiation and/or primer extension, although through different mechanisms. Namely, NNIs binding to the Thumb domain either prevent the Thumb−λ1 loop interaction or interfere with GTP binding.[19,20,25] NNIs binding to the Palm domain may alter the functionality of some key structural and functional elements such as the β-hairpin,[41,42] the C-terminal arm,[42] the catalytic site,[43] and the primer grip.[41] In BVDV, inhibition mechanisms may involve reduction of the Finger flexibility,[40] impairment of translocation of template or products,[40] and disruption of protein−protein interactions.[22]

While NIs have generally a broad spectrum activity (paradigmatic are the 2′-methyl nucleosides, which inhibit growth of Flaviviridae, Picornaviridae, Coronaviridae, and Reoviridae),[44] NNIs are usually specific toward a single genus. In a few cases, they are active against different genera within the same family, as demonstrated by Neyts and co-workers with their imidazo[4,5-*c*]pyridines inhibiting both BVDV and HCV.[40,45,46] However, the molecular reasons behind this behavior have been poorly investigated, in particular as far as the link between the potency of inhibition and binding to homologous or different sites on the RdRps is concerned.

From this perspective, this work focuses on the identification of the targets and the description of the inhibition mechanism of 2-{1-[2-(2,4-dimethoxyphenyl)-1*H*-benzimidazol-5-yl]-ethylidene}hydrazinecarbothioamide [227G[47] (Figure 1)] on both BVDV and HCV. Indeed, 227G is the first benzimidazole derivative endowed with potent and selective activity against both viruses.[47] We integrated biological assays with a thorough computational study, including an extensive protocol for binding site identification and docking, followed by validation using MD simulations and free energy calculations.

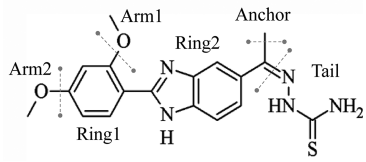

Figure 1. Chemical structure of 2-{1-[2-(2,4-dimethoxyphenyl)-1*H*-benzimidazol-5-yl]ethylidene}hydrazinecarbothioamide (227G), dissected into functional groups.

MATERIALS AND METHODS

Biological. *Cells and Viruses.* Madin-Darby bovine kidney (MDBK) cells were used for the selection of drug-resistant BVDV mutants. Both cells [CCL 22 (NBL-1) *Bos taurus*] and virus (VR-534 strain NADL) were purchased from American Type Culture Collection (ATCC).

Selection of Drug-Resistant Mutants. Drug-resistant variants were selected by serial passages of wild-type (wt) BVDV in the presence of stepwise-doubled 227G concentrations, starting from a cell culture infected with a multiplicity of infection (moi) of 0.01 and treated with a drug concentration equal to the EC_{50}. The amount of virus obtained after each passage was sufficient to determine the level of infection of the next cell culture, which, after infection and washing, was incubated with a double amount of the selecting drug. A 227G-resistant virus population was selected up to a drug concentration 16-fold greater than the EC_{50}. A resistant virus sample was subjected to RNA extraction, reverse transcription polymerase chain reaction (RT-PCR), and genome sequencing to identify the mutation pattern responsible for resistance.

Molecular Analysis of Drug-Resistant Mutants. Viral RNAs from wt and drug-resistant mutants were obtained using the QIAamp viral RNA minikit (Qiagen), starting from 140 μL of cell-free viral suspensions containing ~10^6 plaque-forming units (PFU)/mL. Reverse transcription was conducted using the Superscript II enzyme (Invitrogen), and cDNAs were amplified by PCR using Platinum Pfx polymerase (Invitrogen) following the manufacturer's protocol. Details of the RT-PCR conditions are reported in the Supporting Information.

PCR fragments were purified using the QIAquick PCR purification kit (Qiagen) and analyzed using the cycle-sequencing method (CIBIACI service of the University of Florence, Florence, Italy). Both DNA strands were sequenced with specific primers. The comparative analysis of chromatograms allowed deduction of the mutation pattern responsible for resistance.

Virus Titration by a Plaque Assay. Virus titers of wt BVDV and of 227G-resistant mutant strains, in the absence or presence of the compound, were determined by a plaque reduction assay in infected cell monolayers. MDBK cells were seeded in 24-well plates at a density of 5×10^5 cells/well and allowed to form confluent monolayers by being incubated overnight in growth medium [MEM-Earle's with L-glutamine and 1 mM sodium pyruvate, supplemented with 10% fetal horse serum (FHS)] at 37 °C in a humidified CO_2 (5%) atmosphere.

Monolayers were then infected for 2 h with 250 μL of 1:10 to $1:10^6$ virus dilutions. Following removal of unadsorbed virus, 500 μL of maintenance medium (MEM-Earle's with L-glutamine and 1 mM sodium pyruvate, supplemented with 5% inactivated FBS) was added. Cultures were incubated at 37

dx.doi.org/10.1021/bi400107h | *Biochemistry* 2013, 52, 3752−3764

°C for 4 days and then fixed with PBS containing 50% ethanol and 0.8% crystal violet, washed, and air-dried. Plaques were then counted.

Expression of BVDV NS5BΔ24 Polymerase. Expression and purification of BVDV NS5BΔ24 polymerase were conducted as previously described.[48] Briefly, the expression plasmid encoding the N-terminally His-tagged C-terminal 24-amino-acid-deleted BVDV NS5B was introduced into *Escherichia coli* strain Rosetta 2(DE3)pLysS (Novagene), by chemical transformation. Transformants were then cultured at 30 °C overnight in 5 mL of LB medium containing 25 μg/mL kanamycin and 30 μg/mL chloramphenicol. The culture was diluted into 1 L of LB medium containing 25 μg/mL kanamycin and 30 μg/mL chloramphenicol, incubated at 30 °C until the A_{600} reached 0.6−0.7, and successively induced overnight with 1 mM isopropyl β-D-thiogalactopyranoside. Finally, the cells were harvested by centrifugation and stored at −80 °C until they were purified.

Expression of HCV1b NS5BΔ21 Polymerase. The gene encoding the C-terminal 21-amino-acid-deleted NS5B polymerase (NS5BΔ21) of HCV (BK strain, genotype 1b), C-terminally fused with a six-His tag, was cloned between the BamHI and XhoI cloning sites of the pET-21a(+) expression plasmid (Novagen). The construct encoding the six-His-tagged HCV1b-NS5BΔ21 protein, under the control of the T7 RNA polymerase promoter, was confirmed by dideoxynucleotide sequencing and introduced into *E. coli* strain Rosetta 2(DE3)-pLysS (Novagene) by chemical transformation. A single colony expressing the six-His-tagged HCV1b NS5BΔ21 protein was selected and cultured at 30 °C overnight in 5 mL of LB medium containing 100 μg/mL ampicillin and 30 μg/mL chloramphenicol. The culture was diluted into 1 L of LB medium and incubated at 30 °C until the A_{600} reached 0.6−0.7. The culture was then induced overnight at 25 °C with 1 mM isopropyl β-D-thiogalactopyranoside, and the cells were harvested by centrifugation and stored at −80 °C until they were purified.

Purification of NS5B Proteins. Cell pellets were thawed and immediately lysed by the addition of 10 mL of CelLytic B (Sigma). Any insoluble material was removed by centrifugation at 4 °C and 11000 rpm for 60 min. The soluble extract was applied to a 5 mL column of nickel−nitrilotriacetic acid−agarose (Qiagen), previously equilibrated with lysis buffer [50 mM NaH_2PO_4, 300 mM NaCl, and 10 mM imidazole (pH 8.0)]. The column was washed extensively with wash buffer [50 mM NaH_2PO_4, 300 mM NaCl, and 20 mM imidazole (pH 8.0)], and then the proteins were eluted in a stepwise manner with buffer containing increasing concentrations of imidazole [50 mM NaH_2PO_4, 300 mM NaCl, and 50−250 mM imidazole (pH 8.0)]. The polypeptide composition of the fractions was monitored by Coomassie-stained sodium dodecyl sulfate−polyacrylamide gel electrophoresis analysis. Fractions enriched in pure six-His-tagged NS5B proteins, recovered in the 130−250 mM imidazole eluates, were pooled and dialyzed against buffer containing 25 mM Tris-HCl (pH 7.5), 2.5 mM $MgCl_2$, 1 mM dithiothreitol, and 50% glycerol. The protein concentration was determined by the micro-Bradford method (Bio-Rad), with BSA as the standard. Following dialysis, the purified six-His-tagged HCV1b NS5BΔ21 and six-His-tagged BVDV NS5BΔ24 proteins were divided into aliquots and stored at −80 °C.

RNA-Dependent RNA Polymerase Assays. Enzyme assays were performed, as reported previously,[48] in 96-well plates using 10 μg/mL poly(rC) (GE Healthcare, formerly Amersham Biosciences) as a template, 0.1 μg/mL oligo$(rG)_{12}$ (Invitrogen) as a primer, and 80 μM GTP (Invitrogen) as a substrate, in a 20 μL reaction mixture containing 20 mM Tris-HCl (pH 7.0), 1 mM dithiothreitol, 25 mM NaCl, 20 units/mL RNasin (RNase inhibitor, Promega), 0.5 mM $MnCl_2$ or 5 mM $MgCl_2$, 5% DMSO, 5% glycerol, and 500−600 ng of each purified protein. After preincubation of an enzyme/drug mixture for 30 min at room temperature, reactions were started by the addition of GTP. One microliter of 3-fold serial dilutions of the test compound in 0.5% DMSO, 0.5% DMSO alone as a negative control, or the nucleotide analogue 3′-deoxyguanosine 5′-triphosphate (3′-dGTP) (tebu-bio) as a positive control was added, and the samples were incubated for 120 min at 37 °C (BVDV NS5BΔ24) or 25 °C (HCV1b NS5BΔ21). Reactions were stopped by addition of 2 μL of 200 mM EDTA; 138 μL of the PicoGreen Quantitation Reagent (Molecular Probes), diluted 1:345 in TE, was added to each sample followed by incubation for 5 min at room temperature in the dark. After excitation at 480 nm, the fluorescence was measured at 520 nm in a fluorescence microplate reader (VICTOR^3 Multilabel Plate Reader, Perkin-Elmer). The "relative fluorescence" was calculated by subtracting the mean fluorescence of the blanks and by converting it into the percentage of activity, which was then plotted versus compound concentration.

Dose−response curves were fit with Kaleidagraph (Synergy Software) to obtain the drug concentration providing 50% inhibition (IC_{50}).

Computational. *Molecular Docking. Model Structures for Docking.* X-ray crystal structures of HCV (PDB entries 1CSJ[19] and 2BRK[49]) and BVDV (PDB entry 1S48[21]) RdRps were used as starting models for molecular simulations of the apoenzymes. In HCV, the sequence $_{21}$LPINALSNSLLAHHN$_{35}$ forms a highly flexible loop (λ1), thought to play a major role in ligand−indole/benzimidazole site interactions. This loop is present in 1CSJ,[19] where it folds as an α-helix sitting within a indole/benzimidazole binding site.[49−54] Thus, 1CSJ[19] was used as the starting structure to perform MD simulations of the apoenzyme in this "closed" conformation (hereafter termed APO). However, a starting model was necessary to generate equilibrium conformations of the protein in which the putative binding cavity is not occluded by the λ1 loop. For this purpose, we used structure 2BRK[49] in which λ1 is not resolved. Starting from this structure, we used the Jackal modeling package (http://wiki.c2b2.columbia.edu/honiglab_public/index.php/Software:Jackal) to generate *ex novo* a low-energy conformation of λ1 extending out of the binding site (hereafter termed APO′). This system was used to perform MD simulations from which a representative conformation was extracted to dock 227G.

The RdRp conformations used for docking runs were taken from equilibrium trajectories of APOs by selecting, from the last 20 ns of MD simulations (see below), the structure with the lowest root-mean-square deviation (rmsd) from the average.

The structure of 227G was first drawn with ACD Chem Sketch version 11.0 (http://www.acdlabs.com/resources/freeware/chemsketch). The resulting molecular geometry was then optimized at the B3LYP/6-31G(d,p) level up to a convergence in energy of 10^{-5} au using Gaussian03.[55]

Because no interaction between the HCV or BVDV RdRps and 227G has been reported previously, we searched for putative binding sites on the two enzymes using three different protocols (see Chart 1). First, we exploited the experimental

Chart 1. Docking Protocol[a]

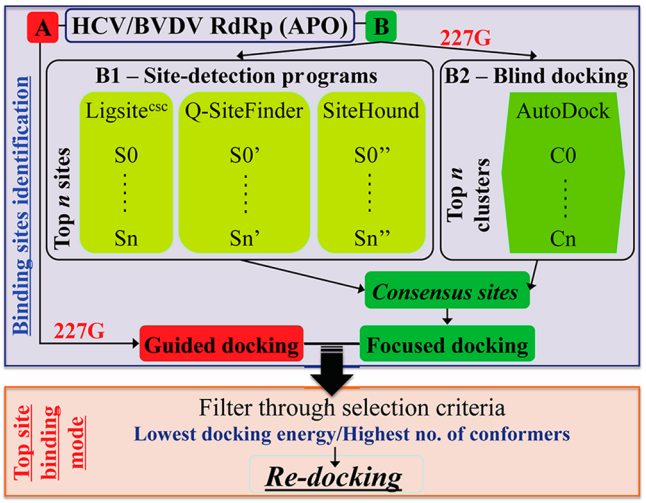

[a]Schematic representation of the protocol used for the identification of binding sites and binding modes of 227G on the HCV and BVDV RdRps.

and computational information[17−20,37−40,49−54] available on the binding of other indole/benzimidazole compounds to each RdRp in guided docking runs (path A in Chart 1). Additionally, we used site detection programs to identify generic binding spots on the enzyme surfaces (path B1 in Chart 1). To assess the robustness of our results, we further performed blind docking calculations (path B2 in Chart 1). On consensus sites, identified by site detection programs and by blind docking, we performed focused docking calculations centering the docking grid on the center of mass of each site detected. Finally, we grouped these poses with those obtained from guided docking. On the highest-affinity site identified in this way, we further ran focused docking ("redocking") calculations, centering the docking grid on the center of mass of 227G in the top pose. All docking runs were performed with AutoDock version 4.0.[56] More details about the docking steps and binding site detection programs are given in the Supporting Information.

MD Simulations. (i) Parametrization. AMBER99SB,[57] AMBER-modified,[58] and TIP3P[59] force fields were used to model proteins, ions, and water, respectively. The GAFF force field[60] was adopted to parametrize 227G after structural relaxation (see above) except for charges, which were derived within the RESP framework[61] from the electrostatic potential map generated by the molecule [calculated with Gaussian03 at the HF/6-31G(d) level[55]].

(ii) MD Setup. All-atom MD simulations were conducted with the NAMD2.8[62] package for the apoenzymes as well as for their complexes with 227G (hereafter termed COM) (Table S1 of the Supporting Information for more details). The solute was placed within a truncated octahedral box (with a 42.9 Å edge length, ensuring a minimal distance of 16 Å between any RdRp atom and the edge of the box) filled with explicit water molecules and counterions. Briefly, geometry optimizations were conducted with a two-step protocol: (i) up to 10000 cycles (2000 of steepest descent and 8000 of conjugate gradient) with harmonic restraint (k = 1 kcal mol^{-1} Å^{-2}) on non-hydrogen atoms of the solute and (ii) up to 10000 conjugate gradient cycles with no restraints. Next, heating to 310 K was achieved by linearly increasing the temperature within 100 ps of *NVT* MD, while imposing restraints of 1 kcal mol^{-1} Å^{-2} on non-hydrogen atoms of the solute. Restraints were then released for 100 ps, and as a last step preceding the productive dynamics, 1 ns of *NPT* MD was conducted to relax the simulation box. Finally, MD simulations with a 30 ns duration for each APO and COM in an explicit water solution under the *NPT* ensemble were performed. Temperature and pressure were regulated at 310 K and 1.013 bar, respectively, using the Langevin thermostat[63] (damping constant of 5 ps^{-1}) and the Nosé−Hoover−Langevin piston pressure control.[64] Electrostatic interactions were evaluated using soft particle mesh Ewald schemes with 1 Å grid spacing and a cutoff of 12 Å, which was used also for Lennard-Jones interactions.

(iii) Analysis of Structure and Energetics. An inventory of structural and energetic features of the complexes was obtained by analyzing the last 20 ns of each MD simulation (i.e., the equilibrated trajectories) in terms of hydrogen bonds (HBs), hydrophobic contacts (HpHs), and water-mediated interactions. The HBs between RdRps and 227G were counted by applying cutoffs of 3.2 Å for the donor−acceptor distance and 150° for the donor−hydrogen−acceptor angle.[65] Durable and transient HBs were defined as those with lifetimes higher and lower than 20% of the MD simulation time, respectively.[65] The formation of alternative HBs between 227G donors or acceptors and surrounding key residues was observed during simulation; therefore, the average dynamic length (ADL) of these contacts was calculated by averaging their distance. A HpH was counted when nonpolar atoms were separated by >4 Å.[65] The cutoff on the short interatomic carbon−carbon distance (SICD), used to calculate $\pi-\pi$ interactions, was set to 4.8 Å.[66] The rmsd per residue wise and the root-mean-square fluctuation (rmsf) were calculated to characterize distortions and changes in protein flexibility. Namely, the rmsd per residue wise was calculated for (a) the average protein structures in COM with respect to their counterparts in APO (to highlight major conformational changes caused by ligand binding) and (b) the average protein structures in APO and COM with respect to crystallographic structures (to assess the presence of major structural differences in MD runs). Finally, the area of the template entrance tunnel during equilibrated dynamics was estimated by considering the triangle defined by terminal residues (Cα) of the loops contributing to the cavity (R127, F224, and A392). The energies of interaction between 227G and key RdRp residues were calculated by summing up the nonbonded (Lennard-Jones and electrostatic) terms of the pairwise molecular mechanics additive function, calculated for the ligand-bound protein and between protein and 227G subgroups.

(iv) MM-PBSA Calculations. To compare the free energies of binding of 227G on HCV and BVDV RdRps, MM-PBSA calculations[67] were performed on 800 snapshots taken from equilibrium trajectories (one every 25 ps). The binding free energy (ΔG_{bind}) of each system was evaluated as follows:

$$\Delta G_{bind} = G_{com} - (G_{rec} + G_{lig}) \quad (1)$$

where G_{com}, G_{rec}, and G_{lig} are the absolute free energies of the complex (RdRp−inhibitor), receptor (RdRp), and ligand (inhibitor), respectively, averaged over the equilibrium trajectory. According to the MM/PBSA method, the free energy difference can be decomposed as $\Delta G = \Delta E_{MM} + \Delta G_{solv} - T\Delta S_{conf}$, where ΔE_{MM} is the difference in molecular mechanics energy, ΔG_{solv} the solvation free energy (including an entropic contribution), and ΔS_{conf} the solute configurational entropy (including the loss of translational and rotational

dx.doi.org/10.1021/bi400107h | *Biochemistry* 2013, 52, 3752−3764

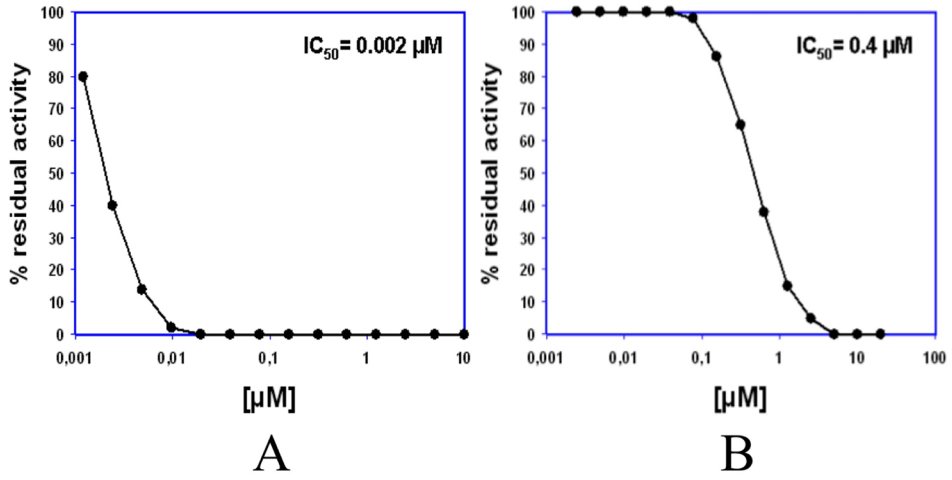

Figure 2. 227G dose–response curves from enzyme assays: (A) BVDV and (B) HCV.

entropy due to binding, as well as changes in the vibrational entropy). The first two terms are calculated with the following equations:

$$\Delta E_{MM} = \Delta E_{bond} + \Delta E_{angle} + \Delta E_{torsion} + \Delta E_{vdw} + \Delta E_{elect} \quad (2)$$

$$\Delta G_{solv} = \Delta G_{PB} + \Delta G_{SA} \quad (3)$$

where E_{MM} includes the molecular mechanics energy contributed by bonded (E_{bond}, E_{angle}, and $E_{torsion}$) and nonbonded (E_{vdw} and E_{elect}) terms of the force field and ΔG_{solv} is the solvation free energy, which has an electrostatic (ΔG_{PB}, evaluated using the Poisson–Boltzmann equation) and a nonpolar contribution ($\Delta G_{SA} = \gamma \Delta SA + b$) proportional to the surface area (ΔSA). The electrostatic solvation free energy was calculated using DELPHI,[68] with dielectric constants of 1 for the solute and 78.5 for the solvent. Atomic radii were taken from PARSE with an additional value of 1.90 Å for phosphorus, while partial charges were taken from the AMBER/GAFF force fields.[57,60] The electrostatic potential was calculated on a cubic lattice with a length equal to 120% of the longest interatomic distance of the protein, using a grid spacing of 0.5 Å. Up to 10000 iteration steps were requested to reach convergence in energy (using the linear form of the PB equation). The surface area in the equation for G_{SA} was calculated using MOLSURF, with γ and b values of 0.00542 kcal mol^{-1} Å^{-2} and 0.92 kcal/mol, respectively, for use with PARSE atomic radii. The solvent probe radius was set to 1.4 Å.

The solute entropy contribution, $-T\Delta S_{conf}$, was estimated by normal mode analysis[67] using the NMODE module of AMBER 9.0. For each snapshot, the structures of the complex, receptor, and ligand were first optimized in the absence of explicit solvent, using a distance-dependent dielectric constant ε of 4r (r is the interatomic distance) to mimic solvent screening. The convergence cutoff on the potential energy gradient was set to 10^{-4} kcal mol^{-1} Å^{-1}. Furthermore, to reduce the error in the evaluation of the entropic term, we adopted a recently developed method[69] in which normal mode calculations were performed on subsets of system atoms, namely on those belonging to the residues within 10 Å of the center of mass of the inhibitor, including water molecules and ions.

To estimate the contribution of key residues to the stability of the complex, the decomposition method implemented in AMBER 11 was applied within the framework of the molecular mechanics (MM) generalized Born surface area (GBSA) approach.[70] In addition to being faster than the MM-PBSA[67] approach, MM-GBSA[70] methods furnish an intrinsically easy way of decomposing the free energy of binding into contributions from single atoms and residues, which is alternative to the "alanine scanning" approach. The electrostatic solvation free energy was calculated using the implicit solvent model in combination with mbondi2 (for H, C, N, O, and S elements) and intrinsic radii. Partial charges were taken from the AMBER/GAFF force fields, and relative dielectric constants of 1 for solute and 78.4 for solvent (0.1 M KCl water solution) were used. The nonpolar contribution is approximated by the LCPO[71] method implemented within the sander module of AMBER 11.

RESULTS

Biological. *Activity in Cell-Based and Enzyme Assays.* As previously reported, 227G (compound **31** in ref 47) showed no cytotoxicity for uninfected MDBK cells at concentrations as high as 100 μM, and an EC_{50} value of 0.80 ± 0.06 μM against BVDV. Moreover, in a replicon assay with human hepatoma cells (GS4.1), 227G selectively inhibited the HCV replication with an EC_{50} of 1.11 ± 0.15 μM.[47] Here, to identify the target of 227G, BVDV and HCV recombinant RdRps were expressed, purified, and evaluated in enzyme assays based on the use of the RiboGreen fluorescent dye to detect transcripts. Dose–response curves indicate that 227G potently inhibits (IC_{50} = 0.0020 ± 0.0004 μM) the BVDV RdRp activity (Figure 2A). Moreover, the drug also inhibits, although with a lower potency (IC_{50} = 0.40 ± 0.04 μM), the HCV recombinant enzyme (Figure 2B).

Molecular Characterization of Drug-Resistant Mutants. To confirm the enzymatic data presented above suggesting the BVDV RdRp as the molecular target of 227G, drug-resistant BVDV mutants were selected by serial passages of the wt strain in the presence of stepwise doubled 227G concentrations, up to a concentration 16-fold greater than the EC_{50}. Replication efficiencies of plaque-purified wt and 227G-resistant mutant strains were then compared in the absence and presence of 12.8 μM 227G. As expected, in the presence of the drug, the yield of the wt strain decreased by more than 3 logs as compared to that in the drug-free medium (1×10^8 PFU/mL). On the other hand, the yield of the drug-resistant mutant was the same in the absence and presence of 227G and on the same order of

dx.doi.org/10.1021/bi400107h | *Biochemistry* 2013, 52, 3752–3764

magnitude (1.4×10^8 PFU/mL) as that of the wt strain grown in drug-free medium, suggesting equivalent *in vitro* fitness.

To identify the mutation pattern responsible for drug resistance, aliquots of wt and mutant viruses were subjected to RNA extraction, RT-PCR, and sequencing of genome regions encoding the nonstructural proteins (NS2−NS3−NS4A−NS4B−NS5A−NS5B) containing the principal enzymes involved in replication. Comparative analysis of the wt and mutant genomes showed, in the latter, a mutation located in the gene encoding the NS5B protein, while no mutations were detected in the genes encoding the other nonstructural proteins. The mutation consists of an A-to-G substitution at nucleotide (NT) 783, which results in the change of an isoleucine to a methionine at amino acid 261. It is worth noting that the I261M mutation, like other mutations responsible for BVDV resistance to other NNIs,[37−40,72−74] is localized in the Finger domain. In contrast, mutations conferring HCV resistance to a variety of NNIs (including benzimidazoles) are located in the Thumb domain.[49−54,75]

Computational. *Docking.* To identify the most likely sites of binding of 227G on HCV and BVDV RdRps, we used the three approaches described in Materials and Methods and shown in Chart 1. First, guided docking (path A in Chart 1) was performed, taking advantage of previous experimental information about RdRp binding sites, coming from structural studies of the complexes of HCV RdRp with various NNIs,[17,20,36,49−54] and from the location of point mutations related to drug resistance in the BVDV RdRp.[37−40] For the HCV RdRp, the Cα atom of residue L30 (on the λ1 loop), which lies in the experimentally determined binding cavity of indole/benzimidazole NNIs,[36,49,51,75,76] was selected as the grid center for docking runs. As with other indole/benzimidazole NNIs, the two highest-scoring 227G poses (endowed with comparable energies and populations) were found within the Thumb domain (Figure 3A and Figure S1A,B of the Supporting Information).

Following path B in Chart 1, blind docking calculations identified four sites (Figures S2A and S3A of the Supporting Information), all of which were reported previously for other compounds.[18,36] The same four binding pockets are also identified by site detection programs (Figure S4 and Table S2 of the Supporting Information). In a manner consistent with guided docking results, top poses were found on site S0 (Figure S2A of the Supporting Information), which again coincided with the indole/benzimidazole binding site.[49,51,75] The consensus binding sites described above were then used as grid centers for focused docking calculations, which further confirmed S0 as the preferred binding site for 227G (Table S2 of the Supporting Information). Finally, the highest-affinity poses on this site obtained via both paths were grouped and ranked according to the docking energy score and cluster population. The top pose was used for refinement calculations by centring the docking grid on the center of mass of 227G in that pose. This "redocking" onto the indole/benzimidazole binding site gave two possible orientations of 227G (hereafter poses 1 and 2) with comparable scores and populations (Figure 3A and Figure S3B of the Supporting Information).

Figure 3A shows the HCV RdRp binding site, which is constituted by subpockets I (residues A395, L425, H428, and F429), II (residues L392, A393, A396, L492, and V494), and III (residues M423, T427, P495, V499, W500, and R503). Here, the 227G tail (absent in other NNIs[49,51]) allows our lead compound to establish extended interactions with subpocket

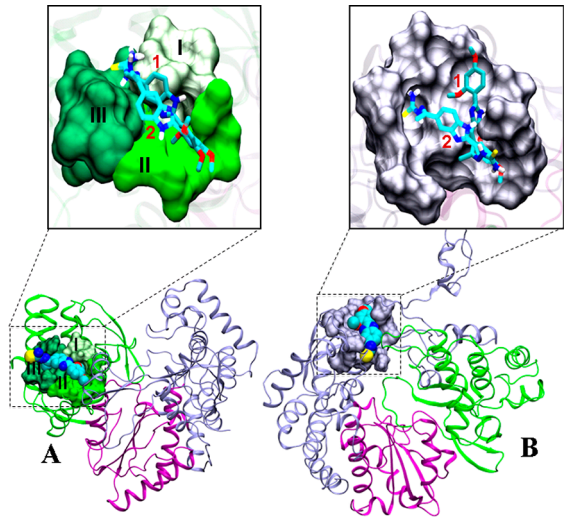

Figure 3. 227G binding sites and poses found by docking. Proteins are shown as ribbons, with Thumb, Finger, and Palm domains colored green, ice blue, and purple, respectively. The molecular surface of residues lining the binding sites is highlighted. 227G is represented with van der Waals spheres colored according to atom type. (A) In HCV RdRp, 227G lies in a pocket within the Thumb domain. Three subpockets [I−III (white, light green, and dark green, respectively)] can be identified. (B) In BVDV RdRp, 227G lies within the Finger domain. Insets show highest-scoring 227G poses 1 and 2 that are represented as solid and transparent sticks, respectively. Note that 1 and 2 have the same orientation only in the HCV RdRp.

III. Binding site residues and orientations of both poses are quite similar, although pose 1 is more stable (Figure S3B and Table S3 of the Supporting Information), as the 227G arms and anchor fit into subpockets better than in pose 2. Indeed, in pose 1, 227G is engaged in a series of hydrophobic interactions with the residues of subpockets I−III, while its arm 1 and anchor are flipped in pose 2, pointing out of the pocket. Additional stability is provided by the polar N1 atom of the 227G benzimidazole moiety, which makes electrostatic interactions mainly with H428 in pose 1. This is reflected in the greater interaction strength of pose 1 with the HCV RdRp (−36.4 kcal/mol) versus that with pose 2 (−31.6 kcal/mol) (Table S3 of the Supporting Information). Although small, this difference has significant consequences in terms of the stability of the two poses (*vide infra*).

With regard to BVDV RdRp, because of the lack of crystallographic data indicating a putative NNI binding site, the proximity of 227G to residues I261, N264, and A392 (on the Finger domain) was considered to be pivotal. In fact, the I261M mutation confers resistance not only to 227G but also to other NNI leads active against BVDV (in combination with mutation N264D[37] or E291G[38]). Also, in this case, guided docking calculations resulted in two almost equivalent 227G orientations within the site lined by the residues listed above (Figure 3B). Blind docking calculations and site detection programs identified three consensus sites (Figures S2B, S3C, and S5 of the Supporting Information). Again, very similar poses were found along paths A and B, and the highest-affinity site along path B coincided with that identified by guided docking (Figure S1C,D and Table S4 of the Supporting Information). Redocking calculations confirmed the possibility for two high-affinity orientations of 227G within the highest-affinity site (Figure 3B and Figures S1C,D and S3D of the

dx.doi.org/10.1021/bi400107h | *Biochemistry* 2013, 52, 3752−3764

Supporting Information). In these poses, 227G sat in the Finger domain with opposite orientations, close to key residues I261, N264, and A392 (Figure S6 of the Supporting Information). Pose 1 featured an interaction energy with the protein larger than that of pose 2 (by ∼11 kcal/mol), almost entirely due to differences in electrostatic interactions (Table S3 of the Supporting Information).

In summary, in each RdRp we found two stable poses of 227G (Figure 3 and Figures S1 and S3B−D of the Supporting Information) matching the following criteria: (1) highest docking energy, (2) largest cluster population, (3a) the presence, in the HCV RdRp−227G complex, of key protein−ligand interactions consistent with those found in published X-ray structures of HCV RdRp in complex with indole/benzimidazole NNIs, and (3b) the proximity, in the BVDV RdRp−227G complex, to residues whose mutation confers resistance to benzimidazole NNIs. The high level of consistency between the guided (path A of Chart 1) and unbiased (path B of Chart 1) docking results supports our suggestion that identified sites are the most likely binding spots for 227G. Because two possible orientations of 227G were found thereon, a total of four conformations were chosen as starting structures for subsequent MD simulations.

MD Simulations. To validate docking poses, a total of seven MD simulations were performed for the HCV and BVDV RdRps in their apo and holo forms (Table S1 of the Supporting Information). Simulations of the apoenzymes (APOs) were conducted to compare the structural and dynamic parameters of the latter with those of the RdRp−227G complexes. In this respect, it should be noted that the structures of both enzymes did not differ appreciably from the corresponding X-ray structures along the full MD simulation (Figure S7 of the Supporting Information). With regard to the complexes, it is worth noticing that MD simulations starting from pose 2 (Figure 3 and Figure S1B,D of the Supporting Information) resulted in unstable complexes, featuring dissociation of 227G from the receptor after a few nanoseconds (data not shown). The remaining simulations (including those of the APOs) were stable and reached a plateau in the total rmsd after ∼10 ns (Figure S8 of the Supporting Information).

In the case of HCV RdRp, only modest structural distortions were found upon binding, in agreement with experimental data.[49−54,75] As expected, the largest difference arises from the partial folding of the λ1 loop into a helical structure in the apoenzyme (Figure S7A of the Supporting Information). Also, in the case of BVDV, global structural changes were modest. In this case, the main differences with respect to the X-ray structure of PDB entry 1S48[21] are localized in the intrinsically more mobile RdRp regions, including the linker loop (Figure S7B of the Supporting Information). If the deviation in APO could be, at least in part, due to the limited conformational freedom experienced by the protein in X-ray crystals, the more drastic conformational changes in COM are likely due to the interaction of the loop with 227G. Given the low rmsd values of both HCV and BVDV APOs with respect to those of their respective X-ray structures, the average structures from those simulations were used as a reference to assess the impact of binding.

HCV RdRp−227G Complex. In its stable pose, 227G sits within the binding cleft of the HCV RdRp Thumb domain (Figure 4A and Figure S9A of the Supporting Information) in a manner similar to that determined by X-ray crystallography for indole derivatives[49,51] (Figure S9B of the Supporting

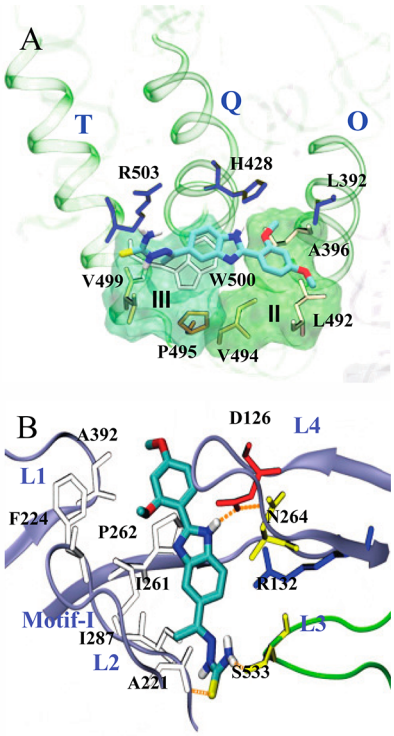

Figure 4. 227G binding modes and interaction maps from MD. Shown are representative MD frames featuring the lowest rmsd with respect to the average structure of the complexes, as extracted from MD trajectories. (A) For HCV RdRp, helices T, Q, and O outlining the cavity are shown in transparent green. Key residues of subpockets II and III (transparent green and light green surfaces, respectively) are also shown, colored according to their chemical characteristics (acidic, basic, HpH, and polar colored red, blue, white, and yellow, respectively). (B) In BVDV RdRp, loops L1−L4 and motif I are shown (the color code is the same as in Figure 3, and key residues are colored as in panel A). For the sake of clarity, residue E128 was omitted. Orange spiral rings indicate HBs involving residues D126, A221, and S533, as well as a salt bridge between D126 and N264.

Information). The binding cavity is mainly hydrophobic and comprises the three closely spaced subpockets [I−III (see Figure 4A and Docking)] and the three α-helices (T, Q, and O) delimiting its back border.

Along the MD trajectory, 227G assumes a slightly different orientation than in docking: it loses contacts with subpocket I and makes stronger interactions with subpockets II and III (Figure S10A of the Supporting Information). The phenyl moiety (ring 1) and the *O*-methyl group (arm 2) of the ligand fully occupy subpocket II, which is partially filled with the side chains of residues L30 and L31 of the λ1 loop in the APO (Figure S9A of the Supporting Information). In particular, the *O*-methyl group, protruding into the pocket more deeply than residues L30 and L31, allows 227G to fit into the cavity better than the λ1 loop. On average, all residues lining subpockets I−III, except A393, are in direct contact with 227G during MD simulations, thus allowing a better packing of 227G within the pocket, documented by a binding energy (by 14.5 kcal/mol) larger than that of the stable docking pose (cf. Tables S3 and S5 of the Supporting Information). The largest contribution is associated with the 227G tail, which is the only portion making significant electrostatic interactions with the binding pocket (Table S5 of the Supporting Information). The benzimidazole moiety (ring 2) interacts with residues V499 and W500 of helix

dx.doi.org/10.1021/bi400107h | *Biochemistry* 2013, 52, 3752−3764

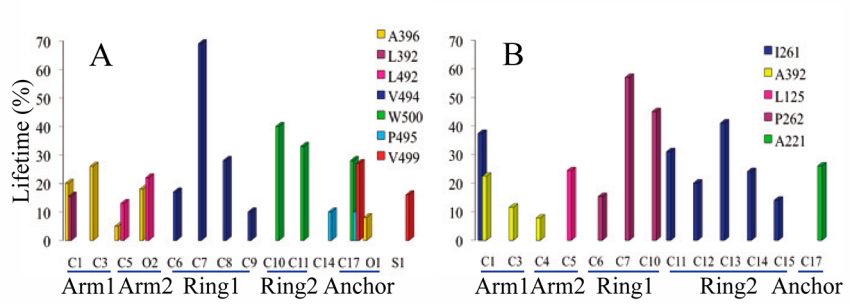

Figure 5. Key hydrophobic ligand−enzyme interactions in (A) HCV and (B) BVDV. The *x*-axis refers to atoms of the 227G functional groups. The *y*-axis refers to the interaction lifetime with the RdRp, reported as a fraction over the entire simulation time. Different colors highlight interactions with different residues of the binding pockets.

T (subpocket III), which are also in contact with the methyl group (anchor), stabilizing 227G in the cavity (Figures 4A and 5A). Noteworthy is the fact that these contacts occur (although transiently) over the whole equilibrium trajectory. Also, the phenyl moiety (ring 1) makes extended and persistent hydrophobic interactions with residue V494 (Figure 5A). Further stabilization comes from $\pi-\pi$ interactions between the benzimidazole moiety and residue W500 and from the hydrophobic contacts with residues L392 and A396 of helix O, L492 of subpocket II, and P495 of subpocket III (Figure 4A).

As expected, the largest protein's structural deviation with respect to the APO is seen in the λ1 loop (Figure S7A of the Supporting Information), which floats out of the pocket in COM. Consistently, also the average flexibility of the RdRp (which increases slightly upon 227G binding) features a peak at the λ1 loop (Figure 6A).

In conclusion, the picture of the 227G−RdRp interaction resulting from this study for HCV is consistent with previous crystallographic and NMR studies performed with other indole- and benzimidazole-based allosteric inhibitors.[36,49−54,75] To further validate the correspondence between *in silico* and experimental results, we evaluated the free energy of binding of 227G to the HCV RdRp using the MM/PBSA approach.[67] Good agreement is obtained (Table 1) between the calculated ΔG_B and that extracted from the IC_{50} value of enzyme assays, supporting the reliability of the 227G binding site identified by molecular modeling and MD simulations. The major source of stabilization comes from hydrophobic interactions (cf. ΔG_{VDW+NP} and ΔG_{ELE+PB} in Table 1). Consistently, all but one of the key residues contributing mostly to the stability of the RdRp−227G complex (Table S6 of the Supporting Information) are hydrophobic, which is also in agreement with the HpH interaction graph (Figure 5A).

Comparison with the BVDV RdRp−227G Complex. Like in HCV, in BVDV the 227G binding region undergoes structural rearrangements with respect to the docking geometry during the MD trajectory (Figure S10B of the Supporting Information). In the stable pose, 227G sits in a cavity encircled by four loops (Figure 4B): L1 (P388−I398) and L2 (A221−N229), which belong to the Finger domain; L3 (L530−G537), which belongs to the Thumb domain; and L4 (L125−R132), also known as the linker, which is part of the N-terminal domain.[21,22] In addition, ring 2 of 227G stacks against motif I (I261−K266), which is located in the flexible Fingertip region. The residues lining the binding pocket are mostly hydrophobic (A221, A222, F224, I261, P262, I287, and A392) and polar (T160, T162, N217, N264, and S533), although three basic

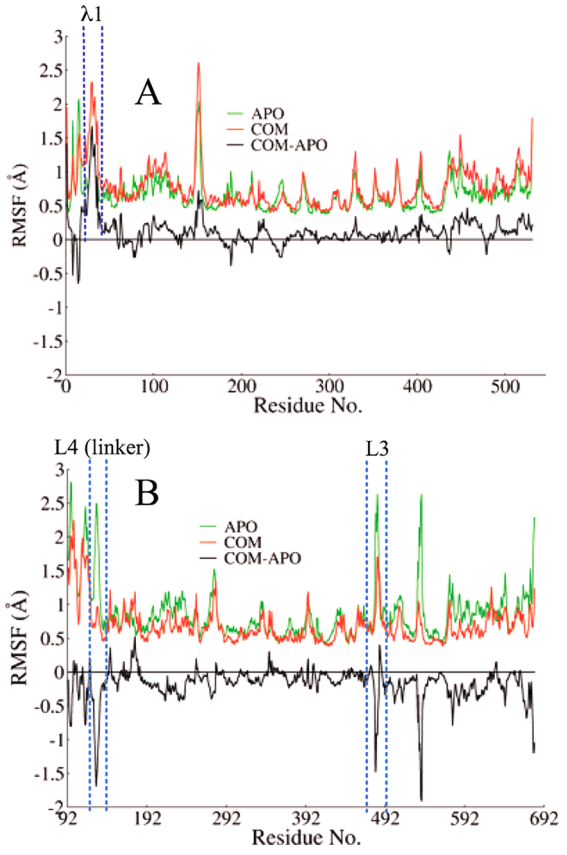

Figure 6. Flexibility of RdRps in their apo and holo forms in HCV (A) and BVDV (B), estimated from the rmsf values along the equilibrium MDs.

(R127, R130, and R132) and two acidic (D126 and E128) residues are present. Some of these residues, namely, N217, A221, A222, and I261M, were also found to interact with other NNIs,[37−39] but most of them are specific to the complex between the polymerase and 227G. In particular, 227G is the only benzimidazole compound interacting with the linker loop of the N-terminal domain.

Like in HCV, the major interactions involve the 227G benzimidazole moiety (ring 2) and tail (Figure 5B and Table S5 of the Supporting Information). A network of inter- and intramolecular HBs further stabilizes 227G in the pocket (Figure 4B and Figure S11 of the Supporting Information). In particular, an HB is established between N2@227G and atoms OD1@D126 and OD2@D126, with an ADL of 2.3 Å and passage of 80% of the simulation time (Table S7 of the

dx.doi.org/10.1021/bi400107h | *Biochemistry* 2013, 52, 3752−3764

Table 1. Experimental and Calculated Free Energies of Binding of 227G to the HCV and BVDV RdRps[a]

	HCV	BVDV
ΔE_{ELE}	−16.8 (2.3)	−25.2 (1.5)
ΔE_{VDW}	−21.9 (1.4)	−47.2 (3.9)
ΔG_{PB}	9.5 (0.9)	44.1 (2.2)
ΔG_{NP}	−3.7 (1.4)	−5.8 (1.7)
PB_{tot}	−32.9 (2.9)	−33.8 (3.8)
ΔG_{ELE+PB}	−7.3 (2.7)	18.2 (3.9)
ΔG_{VDW+NP}	−25.6 (3.1)	−53.0 (5.1)
$-T\Delta S_{conf}$	23.4 (1.8)	18.9 (2.3)
IC_{50}	0.40 (0.04)	0.0020 (0.0004)
ΔG_B[b]	−9.5 (1.8)	−14.0 (3.1)
ΔG_B[c]	−8.7	−12.2

[a]Energies are in kilocalories per mole; IC_{50} values are in micromolar. Experimental ΔG_{bind} values are estimated from IC_{50} data with the equation $\Delta G_{bind} = RT \ln IC_{50}$ (R is the universal gas constant, and T = 298.5 K). Calculated values are given by the formula $\Delta G_{bind} = \Delta E_{ELE} + \Delta E_{VDW} + \Delta G_{PB} + \Delta G_{NP} - T\Delta S_{conf}$. The various contributions are also shown. [b]Calculated values. [c]Experimental values.

Supporting Information), and a transient HB is formed between N5@227G and OG@S533 on the L3 loop. Finally, the complex is stabilized by water-mediated interactions between NH@E128 and N1@227G, which persist along the whole equilibrium trajectory, although the mediating water molecule changes during simulation (Figure S11 of the Supporting Information).

With respect to the HCV enzyme, 227G influences in a more drastic manner both the structure and the dynamics of the BVDV RdRp (see Figure S12 of the Supporting Information). Indeed, the drug induces a distortion of the entire enzyme (the average rmsd value from APO is ∼2.9 Å) more significant than that observed in the HCV RdRp (average value of ∼1.8 Å). Particularly large are the displacements induced in loops L3 and L4 (which are in direct contact with the ligand) and in the hood region (residues V92−R133). Panels A and B of Figure 7 show that all the four loops surrounding the binding pocket "embrace" 227G. These conformational changes result in a dramatic reduction in the entrance area of the RNA template tunnel that in the APO (as well as in the X-ray structure) is large enough to allow passage of the RNA template. The comparison of the template tunnel entrance areas (see Materials and Methods) among the X-ray structure [∼55 Å^2 (Figure 7C)], APO (∼60 Å^2), and COM (∼28 Å^2) gives an indication of the remarkable effect of 227G on the structure of the binding region. This effect is not only structural: indeed, tight binding of 227G reduces the mobility of almost all the BVDV RdRp residues, in contrast to what happens in HCV (Figure 6). The larger impact of 227G on BVDV than on HCV appears to be consistent with the more potent inhibitory activity on the former enzyme. The largest reduction of the mobility is found in the L3 loop and the N-terminal domain, specifically in the L4 loop, whose fluctuation is thought to be crucial for the proper functioning of the RdRp.[21,22]

As for HCV, we further validated the binding mode by comparing the binding free energies extracted from IC_{50} data and calculated with the MM/PBSA method.[67] As shown in Table 1, there is a good agreement between the two values. In this case, four charged and polar residues are among the eight key amino acids mostly contributing to stabilization of the complex (Table S6 of the Supporting Information). Noteworthy is the fact that residue I261, whose mutation is responsible for resistance to 227G and other benzimidazoles[37] and arylazoenamines,[38] has the largest effect (Figure 5B and Table S6 of the Supporting Information).

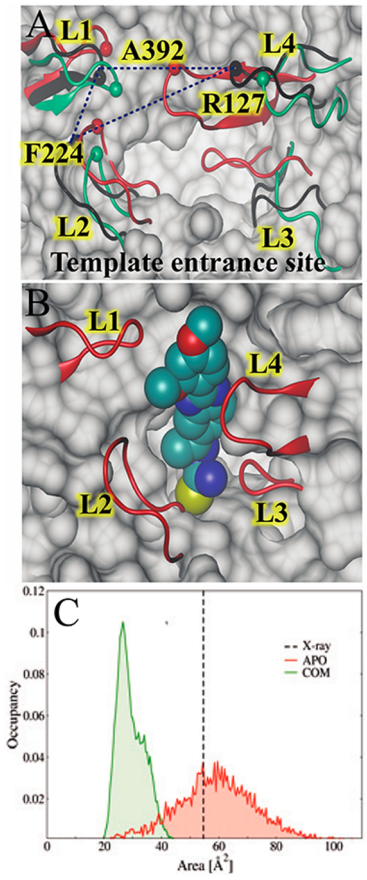

Figure 7. Entrance area of the template tunnel in BVDV. (A) Superimposition of representative structures of the four loops lining the template entrance area in the X-ray (PDB entry 1S48, black), APO (green), and COM (red) structures. Beads correspond to the Cα atoms of residues A392 (loop L1), F224 (loop L2), and R127 (loop L4) used to calculate the template entrance area, as they show the highest variation between the APO and COM. The rest of the protein (X-ray structure) is shown as a gray molecular surface. (B) Same as panel A, but only COM is shown together with 227G, represented with van der Waals spheres. (C) Distribution of the area defined by Cα atoms of residues R127, F224, and A392, as extracted from equilibrium MD simulations of the APO and COM. The black vertical line indicates the value extracted from the X-ray structure (54.6 Å^2).

DISCUSSION

In the context of the rational design and development of new RdRp inhibitors, an NNI active against both BVDV and HCV is a rare finding, as only a few imidazo[4,5-*c*]pyridines are known to be active against both viruses.[45,46] According to our study, 227G is the first benzimidazole NNI active against BVDV and HCV at micromolar concentrations. In cell-based assays, it inhibits the multiplication of both BVDV and HCV with similar potencies. When tested against a wide panel of other RNA and DNA viruses, 227G fails to show broad antiviral activity, thus resulting in a specific inhibitor of viruses representative of the *Pesti* and *Hepaci* genera of the Flaviviridae family. In both cases, the target of 227G appears to be the RdRp. In fact, in enzyme assays, 227G inhibits (although with a different potency) the

dx.doi.org/10.1021/bi400107h | *Biochemistry* 2013, 52, 3752−3764

activity of BVDV and HCV recombinant enzymes. Noteworthy, as far as BVDV is concerned, is the fact that in cell-based assays inhibition occurs at concentrations 500-fold higher than in enzyme assays. Possible explanations could be (i) the lower membrane permeability of the drug, and/or (ii) the greater metabolic instability, and/or (iii) the lower accessibility to the replication complex in BVDV-infected MDBK cells.

To elucidate the molecular reasons for the activity of 227G against the RdRps of both BVDV and HCV, a thorough computational investigation was performed. By combining biased and blind docking with binding site detection programs (cross-validating our findings), we identified two different binding sites on HCV and BVDV RdRps. In the case of HCV, the binding site resides in the same region of the Thumb domain involved in binding of other indole/benzimidazole NNIs,[49,51,75] i.e., the λ1 loop cavity. In the case of BVDV, a novel high-affinity site was found in the Finger domain, at the entrance area of the RNA template tunnel. Interestingly, binding to this site has been recently described for an allosteric inhibitor (an *N*-sulfonyl-anthranilic acid derivative) of the Dengue RdRp.[77]

Although different docking methodologies converged to the same result, further validation was obtained through MD simulations, which account for the role of dynamical motions of the RdRp−227G complexes and of the solvent in the binding process. By adopting MD simulation times much longer than in our previous work,[35] we collected a wider range of statistics of conformations needed for (a) thorough characterization of the structural and dynamical properties of the binding pocket and (b) more reliable calculations of the binding free energy via the MM/PBSA and MM/GBSA approaches.[67,70,78] The need for such validation is evident in this case by considering that, for both RdRp−227G complexes, only one orientation of the drug resulted in stable complexes along multinanosecond MD runs, which clearly points to a strong specificity of 227G interactions within the binding site. In addition, it confirms the importance of explicitly including dynamical motions and solvent effects to identify false positive from docking, as well as to properly assess the stability of receptor−ligand adducts (non-negligible rearrangements leading to optimization of the interactions also occurred for stable poses).[76,79] A further validation of the binding poses comes from the comparison of the calculated affinities of 227G for both enzymes. Indeed, the values of ΔG_B were fairly consistent with the 200-fold greater inhibition potency shown by the compound against the BVDV RdRp than against HCV RdRp.

The concordance between computational and experimental data confers further reliability to our hypothesis of different modes of inhibition of the HCV and BVDV RdRps by 227G. In the case of HCV, inhibition occurs via a mechanism similar to that postulated for other indole- and benzimidazole-based allosteric inhibitors.[36,49−54,75] In APO, the tip of the λ1 loop has an α-helix structure stacking against the Thumb domain and provides to Thumb and Fingers domains the conformational flexibility essential for RNA template translocation, thus favoring RdRp processivity. Therefore, 227G constrains the enzyme into an open, inactive conformation by binding to the Thumb domain and, consequently, by preventing its interaction with the λ1 loop.

In the case of BVDV, we propose an equally articulated mechanism of RdRp inhibition. Here, the 227G binding site is lined with regions that are crucial for proper enzyme functioning. Among them, the N-terminal domain is the most peculiar, being an exclusive region of the RdRps of other Flaviviridae.[21,22,80,81] Although no clear evidence of the role of this domain has yet been given, it is believed that, in combination with the Fingertip region, it forms the entrance of the RNA template tunnel[21,22,81] and its intrinsic movement (along with the Fingertip regions) might drive translocation of the template.[82] The flexibility of these regions could also be very important for template translocation.[19,21] Binding of 227G reduces the entrance area to approximately half of its value in the ligand-free enzyme, because of the convergence of the loops on the ligand. Further occlusion of this tunnel may be due to the size of the drug itself, which stacks onto motif I. Because the latter plays an essential role in binding the incoming NTPs,[21] interaction of 227G with the Fingertip region may prevent this important function. These abundant structural changes also hamper the movements of the Thumb and Finger domains, whose coordination is necessary for template translocation during polymerization.[19] In particular, the dynamics of loops L1−L4 are strongly affected by drug binding. Thus, the intrinsic functional flexibility of the linker (L4), which is thought to escort the template into the catalytic site, is remarkably reduced. In addition, the interaction of 227G with the linker could also weaken its eventual interactions with a second RdRp monomer, thus hindering dimer formation and, consequently, transcription.

■ CONCLUSIONS

In this work, we report the first thorough *in silico* study of an NNI lead active against two viruses, HCV and BVDV, belonging to different genera of the Flaviviridae family. The identification of different binding regions for the same lead on the two RdRp proteins points to the fact that, even if a compound is active against homologous targets, the equivalence of the underlying mechanisms of action cannot be taken for granted. Indeed, the basis for the similar activity of 227G against two viruses apparently lies on its fortuitous capability to bind to two different regions of homologous enzymes causing inhibition of the same process (transcription) through different modes of action. In this respect, 227G exhibits behavior different from that of 2′-methyl nucleosides, capable of inhibiting distantly related virus families that, during evolution, have conserved critical sequences in their RdRp catalytic sites.[19,25]

As a consequence, although BVDV remains a useful surrogate model for identifying new HCV RdRp NIs,[15,48] caution should be applied as far as NNIs are concerned. In fact, the concordance, in terms of the molecular mechanism of action, between drugs capable of inhibiting the replication of both BVDV and HCV is still largely unknown. Thus, as in the case of 227G, inhibition of both BVDV and HCV could be due only to serendipity, and the possibility of starting a successful rational design from data obtained in the surrogate model has to be proven. From this perspective, the inventory of interactions established between 227G and the HCV and BVDV RdRps will be the basis of our structure-based strategy aiming at separately improving the potency of 227G.

■ ASSOCIATED CONTENT

Supporting Information

Additional details regarding primers and parameters used in RT-PCRs; details of guided docking, focused docking, blind docking, and site detection programs; and Figures S1−S12 and

dx.doi.org/10.1021/bi400107h | *Biochemistry* 2013, 52, 3752−3764

Tables S1−S7 as described in the text. This material is available free of charge via the Internet at http://pubs.acs.org.

AUTHOR INFORMATION

Corresponding Author

*S.A.: telephone, +39070 675 4891; e-mail, shailendraasthana@gmail.com. P.R.: telephone, +390706754922; e-mail, paolo.ruggerone@dsf.unica.it. P.L.C.: telephone, +39070 675 4037; 675 4147; e-mail, placolla@unica.it.

Funding

S.A. and S.S. thank MIUR-Direzione Generale per l'Università and Regione Autonoma della Sardegna for financial support via the program "Borse per giovani ricercatori indiani/BOIND04L98", Area Bioinformatica e Neuroinformatica, and RAS-POR FSE 2007-2013, L.R. 7/2007-Progetti di ricerca fondamentale o di base/CRP1_587 "Struttura, funzione ed evoluzione delle RNA polimerasi RNA-dipendenti dei virus". A.V.V. acknowledges financial support from "Regione Autonoma della Sardegna" through a Research Fellow on fundings "PO Sardegna FSE 2007-2013, L.R.7/2007 Promozione della ricerca scientifica e dell'innovazione tecnologica in Sardegna". P.L.C. acknowledges financial support from MIUR-FIRB/RBNE01J3SK ("Development of drugs against Hepaci-, Flavi- and Pesti-viruses"), MIUR/DM 28142 ("Sviluppo di metodologie per la modellizzazione e lo studio di farmaci e biofarmaci"), PON 2006-2009/CYBERSAR ("Cyberinfrastructure per la ricerca scientifica e tecnologica in Sardegna"), and RAS-L.297/99.

Notes

The authors declare no competing financial interest.

ACKNOWLEDGMENTS

Computer time has been provided by CASPUR, CINECA, and CYBERSAR. We acknowledge the technical support of M. Dessalvi.

ABBREVIATIONS

227G, 2-{1-[2-(2,4-dimethoxyphenyl)-1*H*-benzimidazol-5-yl]-ethylidene}hydrazinecarbothioamide; NNI, non-nucleoside inhibitor; NI, nucleoside inhibitor; APO, wild-type enzyme; COM, enzyme−227G complex; HCV, hepatitis C virus; BVDV, bovine viral diarrhea virus; RdRp, RNA-dependent RNA polymerase; NS5B, nonstructural 5B protein; peg-IFN, pegylated interferon; rmsd, root-mean-square deviation; rmsf, root-mean-square fluctuation; PDB, Protein Data Bank; WHO, World Health Organization; AMBER99SB, Amber molecular force field 99SB.

REFERENCES

(1) Hepatitis C, Fact Sheet N°164 (2011) World Health Organization, Geneva (http://www.who.int/mediacentre/factsheets/fs164/en).

(2) Solomon, T., and Mallewa, M. (2001) Dengue and other emerging Flaviviruses. *J. Infect. 42*, 104−115.

(3) Gould, E. A., and Solomon, T. (2008) Pathogenic flaviviruses. *Lancet 371*, 500−509.

(4) Houe, H. (2003) Economic impact of BVDV infection in diaries. *Biologicals 31*, 137−143.

(5) Ghany, M. G., Strader, D. B., Thomas, D. L., and Seeff, L. B. (2009) Diagnosis, management, and treatment of hepatitis C: An update. *Hepatology 49*, 1335−1374.

(6) Bodenheimer, H. C., Lindsay, K. L., Davis, G. L., Lewis, J. H., Thung, S. N., and Seeff, L. B. (1997) Tolerance and efficacy of oral ribavirin treatment of chronic hepatitis C: A multicenter trial. *Hepatology 26*, 473−477.

(7) Sulkowski, M. S. (2003) Anemia in the treatment of hepatitis C virus Infection. *Clin. Infect. Dis. 37*, 315−322.

(8) Sulkowski, M. S., Wasserman, R., Brooks, L., Ball, L., and Gish, R. (2004) Changes in haemoglobin during interferon alpha-2b plus ribavirin combination therapy for chronic hepatitis C virus infection. *Journal of Viral Hepatitis 11*, 243−250.

(9) Poordad, F., McCone, J., Bacon, B. R., Bruno, S., Manns, M. P., and Sulkowski, M. S. (2011) Boceprevir for untreated chronic HCV genotype 1 infection. *N. Engl. J. Med. 364*, 1195−1206.

(10) Bacon, B. R., Gordon, S. C., Lawitz, E., Marcellin, P., Vierling, J. M., and Zeuzem, S. (2011) Boceprevir for previously treated chronic HCV genotype 1 infection. *N. Engl. J. Med. 364*, 1207−1217.

(11) Jacobson, I. M., McHutchison, J. G., Dusheiko, G., Di Bisceglie, A. M., Reddy, K. R., and Bzowej, N. H. (2011) Telaprevir for previously untreated chronic hepatitis C virus infection. *N. Engl. J. Med. 364*, 2405−2416.

(12) Zeuzem, S., Andreone, P., Pol, S., Lawitz, E., Diago, M., and Roberts, S. (2011) Telaprevir for retreatment of HCV infection. *N. Engl. J. Med. 364*, 2417−2428.

(13) Kronenberger, B., and Zeuzem, S. (2009) Current and future treatment options for HCV. *Ann. Hepatol. 8*, 103−112.

(14) Geiss, B. J., Stahla, H., Hannah, A. M., Gari, H. H., and Keenan, S. M. (2009) Focus on flaviviruses: Current and future drug targets. *Future Med. Chem. 1*, 327−344.

(15) Finkielsztein, L. M., Moltrasio, G. Y., Caputto, M. E., Castro, E. F., Cavallaro, L. V., and Moglioni, A. G. (2010) What is Known About the Antiviral Agents Active Against Bovine Viral Diarrhea Virus (BVDV)? *Curr. Med. Chem. 23*, 2933−2955.

(16) De Francesco, R., and Carfí, A. (2007) Advances in the development of new therapeutic agents targeting the NS3−4A serine protease or the NS5B RNA-dependent RNA polymerase of the hepatitis C virus. *Adv. Drug Delivery Rev. 59*, 1242−1262.

(17) De Francesco, R., and Migliaccio, G. (2005) Challenges and successes in developing new therapies for hepatitis C. *Nature 436*, 953−960.

(18) Haudecoeur, R., Ahmed-Belkacem, A., Yi, W., Fortuné, A., Brillet, R., Belle, C., Nicolle, E., Pallier, C., Pawlotsky, J. M., and Boumendjel, A. (2011) Discovery of naturally occurring aurones that are potent allosteric inhibitors of hepatitis C virus RNA-dependent RNA polymerase. *J. Med. Chem. 54*, 5395−5402.

(19) Bressanelli, S., Tomei, L., Roussel, A., Incitti, I., Vitale, R. L., Mathieu, M., De Francesco, R., and Rey, F. A. (1999) Crystal structure of the RNA-dependent RNA polymerase of hepatitis C virus. *Proc. Natl. Acad. Sci. U.S.A. 96*, 13034−13039.

(20) Chinnaswamy, S., Yarbrough, I., Palaninathan, S., R. Kumar, C. T., Vijayaraghavan, V., Demeler, B., Lemon, S. M., Sacchettini, J. C., and Kao, C. C. (2008) A locking mechanism regulates RNA synthesis and host protein interaction by the hepatitis C virus polymerase. *J. Biol. Chem. 283*, 20535−20546.

(21) Choi, K. H., Groarke, J. M., Young, D. C., Kuhn, R. J., Smith, J. L., Pevear, D. C., and Rossmann, M. G. (2004) The structure of the RNA-dependent RNA polymerase from bovine viral diarrhea virus establishes the role of GTP in de novo initiation. *Proc. Natl. Acad. Sci. U.S.A. 101*, 4425−4430.

(22) Choi, K. H., Gallei, A., Becher, P., and Rossmann, M. G. (2006) The structure of bovine viral diarrhea virus RNA-dependent RNA polymerase and its amino-terminal domain. *Structure 14*, 1107−1113.

(23) Kronenberger, B., and Zeuzem, S. (2008) Future treatment options for HCV: Double, triple, what is the optimal combination? *Best Pract. Res., Clin. Gastroenterol. 22*, 1123−1136.

(24) Einav, S., Dvory-Sobol, D. S., Gehrig, E., and Glenn, J. S. (2010) The Hepatitis C Virus (HCV) NS4B RNA Binding Inhibitor Clemizole Is Highly Synergistic with HCV Protease Inhibitors. *J. Infect. Dis. 202*, 65−74.

(25) Bressanelli, S., Tomei, L., Rey, F. A., and De Francesco, R. (2002) Structural analysis of the hepatitis C virus RNA polymerase in complex with ribonucleotides. *J. Virol. 76*, 3482−3492.

(26) Sommadossi, J. P., and La Colla, P. (Novirio Pharmaceuticals Ltd. and Università degli Studi di Cagliari) (2001) Methods and compositions using modofied nucleosides for treating Flaviviruses and Pestiviruses. WO 2001092282.
(27) Sommadossi, J. P., and La Colla, P. (Novirio Pharmaceuticals Ltd. and Università degli Studi di Cagliari) (2001) Preparation of antiviral nucleosides and methods for treating hepatitis C virus. WO 2001090121.
(28) Carroll, S. S., LaFemina, R. L., Hall, D. L., Himmelberger, A. L., Kuo, L. C., MacCoss, M., Olsen, D. B., Rutkowski, C. A., Tomassini, J. E., An, H., Bhat, B., Dan Cook, P., Eldrup, A. B., Guinosso, C. J., Prhavc, M., and Prakash, T. P. (Merck and Co., Inc., and Isis Pharmaceuticals, Inc.) (2002) Preparation of nucleoside derivatives as inhibitors of RNA-dependent RNA viral polymerase. WO 2002057425.
(29) Eldrup, A. B., Allerson, C. R., Bennet, C. F., Bera, S., Bhat, B., Bhat, N., Bosserman, M. R., Brooks, J., Burlein, C., Carroll, S. S., Cook, P. D., Getty, K. L., MacCoss, M., McMasters, D. R., Olsen, D. B., Prakash, T. P., Prhavc, M., Song, Q., Tomassini, J. E., and Xia, J. (2004) Structure-activity relationship of purine ribonucleosides for inhibition of hepatitis C virus RNA-dependent RNA polymerase. *J. Med. Chem. 47*, 2283−2295.
(30) Eldrup, A. B., Prhavc, M., Brooks, J., Bhat, B., Prakash, T. P., Song, Q., Bera, S., Bhat, N., Dande, P., Cook, P. D., Bennett, C. F., Carroll, S. S., Ball, R. G., Bosserman, M., Burlein, C., Colwell, L. F., Fay, J. F., Flores, O. A., Getty, K., LaFemina, R. L., Leone, J., MacCoss, M., McMasters, D. R., Tomassini, J. E., Von Langen, D., Wolanski, B., and Olsen, D. B. (2004) Structure-activity relationship of heterobase-modified 2′-C-methyl ribonucleosides as inhibitors of hepatitis C virus RNA replication. *J. Med. Chem. 47*, 5284−5297.
(31) Tomei, L., Altamura, S., Paonessa, G., De Francesco, R., and Migliaccio, G. (2005) HCV antiviral resistance: The impact of in vitro studies on the development of antiviral agents targeting the viral NS5B polymerase. *Antiviral Chem. Chemother. 16*, 225−245.
(32) Koev, G., and Kati, W. (2008) The emerging field of HCV drug resistance. *Expert Opin. Invest. Drugs 17*, 303−319.
(33) Shi, S. T., Herlihy, K. J., Graham, J. P., Nonomiya, J., Rahavendran, S. V., Skor, H., Irvine, R., Binford, S., Tatlock, J., Li, H., Gonzalez, J., Linton, A., Patick, A. K., and Lewis, C. (2009) Preclinical Characterization of PF-00868554, a Potent Nonnucleoside Inhibitor of the Hepatitis C Virus RNA-Dependent RNA Polymerase. *Antimicrob. Agents Chemother. 53*, 2544−2552.
(34) Legrand-Abravanel, F., Nicot, F., and Izopet, J. (2010) New NS5B polymerase inhibitors for hepatitis C. *Expert Opin. Invest. Drugs 19*, 963−975.
(35) Rydberg, E., Cellucci, A., Bartholomew, L., Mattu, M., Barbato, G., Ludmerer, S. W., Graham, D. J., Altamura, S., Paonessa, G., De Francesco, R., Migliaccio, G., and Carfi, A. (2009) Structural basis for resistance of the genotype 2b hepatitis C virus NS5B polymerase to site A non-nucleoside inhibitors. *J. Mol. Biol. 390*, 1048−1059.
(36) Betzi, S. P., Eydoux, C. C., Bussetta, C. C., Blemont, M., Leyssen, P., Debarnot, C., Ben-Rahou, M., Haiech, J., Hibert, M., Gueritte, F. O., Grierson, D. S., Romette, J. L., Guillemot, J. C., Neyts, J., Alvarez, K., Morelli, X., Dutartre, H., and Canard, B. (2009) Identification of allosteric inhibitors blocking the hepatitis C virus polymerase NS5B in the RNA synthesis initiation step. *Antiviral Res. 84*, 48−59.
(37) Tonelli, M., Simone, M., Tasso, B., Novelli, F., Boido, V., Sparatore, F., Paglietti, G., Pricl, S., Giliberti, G., Blois, S., Ibba, C., Sanna, G., Loddo, R., and La Colla, P. (2010) Antiviral activity of benzimidazole derivatives. II. Antiviral activity of 2-phenylbenzimidazole derivatives. *Bioorg. Med. Chem. 18*, 2937−2953.
(38) Giliberti, G., Ibba, C., Marongiu, E., Loddo, R., Tonelli, M., Boido, V., Laurini, E., Posocco, P., Fermeglia, M., and Pricl, S. (2010) Synergistic experimental/computational studies on arylazoenamine derivatives that target the bovine viral diarrhea virus RNA-dependent RNA polymerase. *Bioorg. Med. Chem. 18*, 6055−6068.
(39) Castro, E. F., Fabian, L. E., Caputto, M. E., Gagey, D., Finkielsztein, L. M., Moltrasio, G. Y., Moglioni, A. G., Campos, R. H., and Cavallaro, L. V. (2011) Inhibition of Bovine Viral Diarrhea Virus RNA Synthesis by Thiosemicarbazones Derived from 5,6-Dimethoxy-1-Indanone. *J. Virol. 85*, 5436−5445.
(40) Paeshuyse, J., Leyssen, P., Mabery, E., Boddeker, N., Vrancken, R., Froeyen, M., Ansari, I. H., Dutartre, H., Rozenski, J., Gil, L. H., Letellier, C., Lanford, R., Canard, B., Koenen, F., Kerkhofs, P., Donis, R. O., Herdewijn, P., Watson, J., De Clercq, E., Puerstinger, G., and Neyts, J. (2006) A Novel, Highly Selective Inhibitor of Pestivirus Replication That Targets the Viral RNA-Dependent RNA Polymerase. *J. Virol. 80*, 149−160.
(41) Chinnaswamy, S., Cai, H., and Kao, C. (2010) An update on small molecule inhibitors of the HCV NS5B polymerase: Effects on RNA synthesis *in vitro* and in cultured cells, and potential resistance in viral quasispecies. *Virus Adapt. Treat. 2*, 73−89.
(42) Le Pogam, S., Kang, H., Harris, S. F., Leveque, V., Giannetti, A. M., Ali, S., Jiang, W. R., Rajyaguru, S., Tavares, G., Oshiro, C., Hendricks, T., Klumpp, K., Symons, J., Browner, M. F., Cammack, N., and Najera, I. (2006) Selection and characterization of replicon variants dually resistant to thumb- and palm-binding nonnucleoside polymerase inhibitors of the hepatitis C virus. *J. Virol. 80*, 6146−6154.
(43) Harrus, D. B., Ahmed-el-Sayed, N., Simister, P. C., Miller, S., Triconnet, M., Hagedorn, C. H., Mahias, K., Rey, F. L. A., Astier-Gin, T. R. S., and Bressanelli, S. P. (2010) Further insights into the roles of GTP and the C terminus of the hepatitis C virus polymerase in the initiation of RNA synthesis. *J. Biol. Chem. 285*, 32906−32918.
(44) Benzaria, S., Bardiot, D., Bouisset, T., Counor, C., Rabeson, C., Pierra, C., Storer, R., Loi, A. G., Cadeddu, A., Mura, M., Musiu, C., Liuzzi, M., Loddo, R., Bergelson, S., Bichko, V., Bridges, E., Cretton-Scott, E., Mao, J., Sommadossi, J. P., Seifer, M., Standring, D., Tausek, M., Gosselin, G., and La Colla, P. (2007) 2′-C-Methyl branched pyrimidine ribonucleoside analogues: Potent inhibitors of RNA virus replication. *Antiviral Chem. Chemother. 18*, 225−242.
(45) Puerstinger, G., Paeshuyse, J., De Clercq, E., and Neyts, J. (2007) Antiviral 2,5-disubstituted imidazo[4,5-c]pyridines: From anti-pestivirus to anti-hepatitis C virus activity. *Bioorg. Med. Chem. Lett. 17*, 390−393.
(46) Puerstinger, G., Paeshuyse, J., Heinrich, S., Mohr, J., Schraffl, N., De Clercq, E., and Neyts, J. (2007) Antiviral 2,5-disubstituted imidazo[4,5-c]pyridines: Further optimization of anti-hepatitis C virus activity. *Med. Chem. Lett. 17*, 5111−5114.
(47) Vitale, G., Corona, P., Loriga, M., Carta, A., Paglietti, G., Giliberti, G., Sanna, G., Farci, P., Marongiu, M. E., and La Colla, P. (2012) 5-Acetyl-2-arylbenzimidazoles as antiviral agents. Part 4. *Eur. J. Med. Chem. 53*, 83−97.
(48) Zhang, N., Liu, Z., Han, Q., Qiu, J., Chen, J., Zhang, G., Li, Z., Lou, S., and Li, N. (2011) Development of one-step SYBR Green real-time RT-PCR for quantifying bovine viral diarrhea virus type-1 and its comparison with conventional RT-PCR. *Virol. J. 8*, 374.
(49) Di Marco, S., Volpari, C., Tomei, L., Altamura, S., Harper, S., Narjes, F., Koch, U., Rowley, M., De Francesco, R., Migliaccio, G., and Carfi, A. (2005) Interdomain Communication in Hepatitis C Virus Polymerase Abolished by Small Molecule Inhibitors Bound to a Novel Allosteric Site. *J. Biol. Chem. 280*, 29765−29770.
(50) Kukolj, G., McGibbon, G. A., McKercher, G., Marquis, M., Lefobvre, S., Thauvette, L., Gauthier, J., Goulet, S., Poupart, M. A., and Beaulieu, P. L. (2005) Binding Site Characterization and Resistance to a Class of Non-nucleoside Inhibitors of the Hepatitis C Virus NS5B Polymerase. *J. Biol. Chem. 280*, 39260−39267.
(51) Ikegashira, K., Oka, T., Hirashima, S., Noji, S., Yamanaka, H., Hara, Y., Adachi, T., Tsuruha, J., Doi, S., Hase, Y., Noguchi, T., Ogura, I. N., Ikeda, S., and Hashimoto, H. (2006) Discovery of conformationally constrained tetracyclic compounds as potent hepatitis C virus NS5B RNA polymerase inhibitors. *J. Med. Chem. 49*, 6950−6953.
(52) LaPlante, S. R., Gillard, J. R., Jakalian, A., Aubry, N., Coulombe, R., Brochu, C., Tsantrizos, Y. S., Poirier, M., Kukolj, G., and Beaulieu, P. L. (2010) Importance of Ligand Bioactive Conformation in the Discovery of Potent Indole-Diamide Inhibitors of the Hepatitis C Virus NS5B. *J. Am. Chem. Soc. 132*, 15204−15212.

(53) Beaulieu, P. L., Gillard, J., Jolicoeur, E., Duan, J., Garneau, M., Kukolj, G., and Poupart, M. A. (2011) From benzimidazole to indole-5-carboxamide Thumb Pocket I inhibitors of HCV NS5B polymerase. Part 1: Indole C-2 SAR and discovery of diamide derivatives with nanomolar potency in cell-based subgenomic replicons. *Bioorg. Med. Chem. Lett. 21*, 123658−123663.
(54) LaPlante, S. R., Jakalian, A., Aubry, N., Bousquet, Y., Ferland, J. M., Gillard, J., Lefebvre, S., Poirier, M., Tsantrizos, Y. S., Kukolj, G., and Beaulieu, P. L. (2004) Binding Mode Determination of Benzimidazole Inhibitors of the Hepatitis C Virus RNA Polymerase by a Structure and Dynamics Strategy. *Angew. Chem., Int. Ed. 43*, 4306−4311.
(55) Frisch, M. J., Trucks, G. W., Schlegel, H. B., Scuseria, G. E., Robb, M. A., Cheeseman, J. R., Montgomery, J. A., Jr., Vreven, T., Kudin, K. N., and Burant, J. C. (2004) *Gaussian*, revision C.02, Gaussian, Inc., Wallingford, CT.
(56) Morris, G. M., Huey, R., Lindstrom, W., Sanner, M. F., Belew, R. K., Goodsell, D. S., and Olson, A. J. (2009) AutoDock4 and AutoDockTools4: Automated docking with selective receptor flexibility. *J. Comput. Chem. 30*, 2785−2791.
(57) Hornak, V., Abel, R., Okur, A., Strockbine, B., Roitberg, A., and Simmerling, C. (2006) Comparison of multiple Amber force fields and development of improved protein backbone parameters. *Proteins: Struct., Funct., Genet. 3*, 712−725.
(58) Joung, I. S., and Cheatham, T. E. (2008) Determination of Alkali and Halide Monovalent Ion Parameters for Use in Explicitly Solvated Biomolecular Simulations. *J. Phys. Chem. B 112*, 9020−9041.
(59) Jorgensen, W. L., Chandrasekhar, J., Madura, J. D., Impey, R. W., and Klein, M. L. (1983) Comparison of simple potential functions for simulating liquid water. *J. Chem. Phys. 79*, 926−935.
(60) Wang, J., Wolf, R. M., Caldwell, J. W., Kollman, P. A., and Case, D. A. (2004) Development and testing of a general amber force field. *J. Comput. Chem. 25*, 1157−1174.
(61) Bayly, C. I., Cieplak, P., Cornell, W., and Kollman, P. A. (1993) A well-behaved electrostatic potential based method using charge restraints for deriving atomic charges: The RESP model. *J. Phys. Chem. 97*, 10269−10280.
(62) Phillips, J. C., Rosemary, B., Wang, W., Gumbart, J., Tajkhorshid, E., Villa, E., Chipot, C., Skeel, R. D., Kale, L., and Schulten, K. (2005) Scalable molecular dynamics with NAMD. *J. Comput. Chem. 26*, 1781−1802.
(63) Izaguirre, J. A., Catarello, D. P., Wozniak, J. M., and Skeel, R. D. (2001) Langevin stabilization of molecular dynamics. *J. Chem. Phys. 114*, 2090−2098.
(64) Feller, S., Zhang, Y. H., Pastor, R., and Brooks, B. R. (1995) Constant-pressure molecular-dynamics simulation: The langevin piston method. *J. Chem. Phys. 103*, 4613−4621.
(65) Kumar, A., Hajjar, E., Ruggerone, P., and Ceccarelli, M. (2010) Molecular Simulations Reveal the Mechanism and the Determinants for Ampicillin Translocation through OmpF. *J. Phys. Chem. B 114*, 9608−9616.
(66) Hunter, C. A., Singh, J., and Thornton, J. M. (1991) π-π interactions: The geometry and energetics of phenylalanine-phenylalanine interactions in proteins. *J. Mol. Biol. 218*, 837−846.
(67) Kollman, P. A., Massova, I., Reyes, C., Kuhn, B., Huo, S., Chong, L., Lee, M., Lee, T., Duan, Y., Wang, W., Donini, O., Cieplak, P., Srinivasan, J., Case, D. A., and Cheatham, T. E. (2000) Calculating Structures and Free Energies of Complex Molecules: Combining Molecular Mechanics and Continuum Models. *Acc. Chem. Res. 33*, 889−897.
(68) Rocchia, W., Sridharan, S., Nicholls, A., Alexov, E., Chiabrera, A., and Honig, B. (2002) Rapid grid-based construction of the molecular surface and the use of induced surface charge to calculate reaction field energies: Applications to the molecular systems and geometric objects. *J. Comput. Chem. 23*, 128−137.
(69) Kongsted, J., and Ryde, U. (2009) An improved method to predict the entropy term with the MM/PBSA approach. *J. Comput.-Aided Mol. Des. 23*, 63−71.
(70) Vargiu, A. V., and Nikaido, H. (2012) Multidrug binding properties of the AcrB efflux pump characterized by molecular dynamics simulations. *Proc. Natl. Acad. Sci. U.S.A. 109*, 20637−20642.
(71) Weiser, J., Shenkin, P. S., and Still, W. C. (1999) Approximate atomic surfaces from linear combinations of pairwise overlaps (LCPO). *J. Comput. Chem. 20*, 217−230.
(72) Baginski, S. G., Pevear, D. C., Seipel, M., Sun, S. C. C., Benetatos, C. A., Chunduru, S. K., Rice, C. M., and Collett, M. S. (2000) Mechanism of action of a pestivirus antiviral compound. *Proc. Natl. Acad. Sci. U.S.A. 97*, 7981−7986.
(73) Sun, J. H., Lemm, J. A., O'Boyle, D. R., Racela, J., Colonno, R., and Gao, M. (2003) Specific Inhibition of Bovine Viral Diarrhea Virus Replicase. *J. Virol. 77*, 6753−6760.
(74) Paeshuyse, J., Chezal, J. M., Froeyen, M., Leyssen, P., Dutartre, H., Vrancken, R., Canard, B., Letellier, C., Li, T., Mittendorfer, H., Koenen, F., Kerkhofs, P., De Clercq, E., Herdewijn, P., Puerstinger, G., Gueiffier, A., Chavignon, O., Teulade, J. C., and Neyts, J. (2007) The Imidazopyrrolopyridine Analogue AG110 Is a Novel, Highly Selective Inhibitor of Pestiviruses That Targets the Viral RNA-Dependent RNA Polymerase at a Hot Spot for Inhibition of Viral Replication. *J. Virol. 81*, 11046−11053.
(75) Tomei, L., Altamura, S., Bartholomew, L., Biroccio, A., Pacini, A. L., Narjes, F., Gennari, N., Bisbocci, M., Incitti, I., Orsatti, L., Harper, S., Stansfield, I., Rowley, M., De Francesco, R., and Migliaccio, G. (2003) Mechanism of action and antiviral activity of benzimidazole-based allosteric inhibitors of the hepatitis C virus RNA-dependent RNA polymerase. *J. Virol. 77*, 13225−13231.
(76) Ma, B., Shatsky, M., Wolfson, H. J., and Nussinov, R. (2002) Multiple diverse ligands binding at a single protein site: A matter of pre-existing populations. *Protein Sci. 11*, 184−197.
(77) Niyomrattanakit, P., Chen, Y. L., Dong, H., Yin, Z., Qing, M., Glickman, J. F., Lin, K., Mueller, D., Voshol, H., Lim, J. Y., Nilar, S., Keller, T. H., and Shi, P. Y. (2010) Inhibition of Dengue Virus Polymerase by Blocking of the RNA Tunnel. *J. Virol. 84*, 5678−5686.
(78) Collu, F., Vargiu, V. A., Dreier, J., Cascella, M., and Ruggerone, P. (2012) Recognition of Imipenem and Meropenem by the RND-Transporter MexB Studied by Computer Simulations. *J. Am. Chem. Soc. 134*, 19146−19158.
(79) Spyrakis, F., BidonChanal, A., Barril, X., and Luque, F. J. (2011) Protein flexibility and ligand recognition: Challenges for molecular modeling. *Curr. Top. Med. Chem. 11*, 192−210.
(80) Lai, V. C. H., Kao, C. C., Ferrari, E., Park, J., Uss, A. S., Wright-Minogue, J., Hong, Z., and Lau, J. Y. N. (1999) Mutational Analysis of Bovine Viral Diarrhea Virus RNA-Dependent RNA Polymerase. *J. Virol. 73*, 10129−10136.
(81) Xiao, M., Li, H., Wang, Y., Wang, X., Wang, W., Peng, J., Chen, J., and Li, B. (2006) Characterization of the N-terminal domain of classical swine fever virus RNA-dependent RNA polymerase. *J. Gen. Virol. 87*, 347−356.
(82) Choi, K. H., and Rossmann, M. G. (2009) RNA-dependent RNA polymerases from Flaviviridae. *Curr. Opin. Struct. Biol. 19*, 746−751.